Quantum Control and Sensing of Nuclear Spins by Electron Spins under Power Limitations

Nati Aharon,[1] Ilai Schwartz,[2] and Alex Retzker[1]
[1]Racah Institute of Physics, The Hebrew University of Jerusalem, Jerusalem 91904, Givat Ram, Israel
[2]NVision imaging, Ulm D-89069, Germany

(Received 6 August 2018; revised manuscript received 2 December 2018; published 29 March 2019)

State of the art quantum sensing experiments targeting frequency measurements or frequency addressing of nuclear spins require one to drive the probe system at the targeted frequency. In addition, there is a substantial advantage to performing these experiments in the regime of high magnetic fields, in which the Larmor frequency of the measured spins is large. In this scenario we are confronted with a natural challenge of controlling a target system with a very high frequency when the probe system cannot be set to resonance with the target frequency. In this contribution we present a set of protocols that are capable of confronting this challenge, even at large frequency mismatches between the probe system and the target system, both for polarization and for quantum sensing.

DOI: 10.1103/PhysRevLett.122.120403

Introduction.—Nuclear spins control by electrons is ubiquitous in quantum technology setups. Control experiments of nuclei in solids were realized via defects in diamond [1,2], especially Nitrogen-Vacancy (NV) centers in diamond [3–7], silicon carbide [8,9], and silicon [10,11]. These experiments were motivated by quantum computing [12–16], quantum sensing [17–19], and dynamical nuclear polarization [20–25]. Nuclear spins control requires one to work at resonance, which is manifested by the Hartmann-Hahn (HH) condition [26]. The HH condition requires one to equate the Rabi frequency (RF) at which the electron is driven to the Larmor frequency (LF) of the nuclei [Fig. 1(a)]. There is, however, a strong motivation to perform experiments at high magnetic fields due to the prolonged nuclear coherence time and the improvement in single-shot readout. Such experiments are very challenging and only a few were realized successfully [17,27–29]. Moreover, in some experiments (e.g., in biological environments) the maximal RF is restricted by deleterious heating effects that are associated with high power. In such cases it is challenging to reach the high RF that matches the nuclear LF [Fig. 1(b)].

In this Letter we present a few schemes that can overcome this limitation in the various regimes of the mismatch between the RF and the targeted LF. We show that by employing a detuned driving field with a constant bounded RF or a driving field with a (bounded) modulated RF or a modulated phase, it is possible to reach the HH condition [Fig. 1(c)]. Although such protocols were achieved with pulsed schemes that require high power [30], we introduce simpler continuous drive based constructions that are significantly more power efficient [31,32]. While we focus on the NV center, the presented schemes are general and applicable to both the optical and microwave domains, and hence to a variety of atomic and solid state systems.

The model.—We consider an NV center electronic spin that is interacting with a single or several nuclei via the dipole-dipole interaction. Under an on-resonance drive, the Hamiltonian of the NV and a nuclear spin is given by [33] $H=(\omega_0/2)\sigma_z+(\omega_l/2)I_z+g\sigma_z I_x+\Omega_1\sigma_x\cos(\omega_0 t)$,

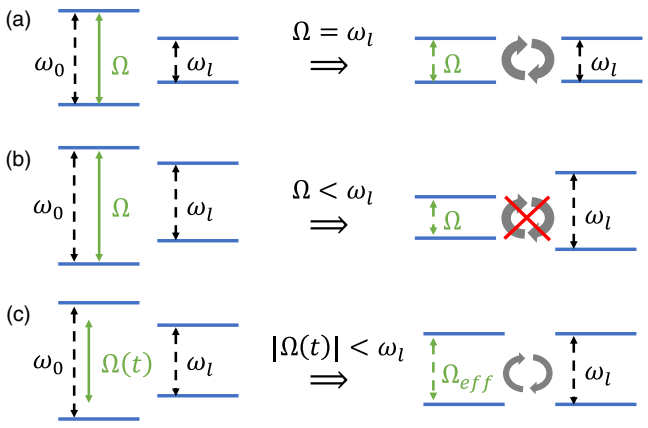

FIG. 1. The main problem. (a) Control and sensing of nuclear spins is achieved by satisfying the HH condition. The electron is driven with a RF (Ω) that is equal to the nuclear LF (ω_l). This results in dressed electron states that are on resonance with the LF, enabling the electron-nucleus spin interaction. (b) The electron is driven with a bounded RF, which is smaller than the LF ($\Omega < \omega_l$) and thus no coupling can be achieved. This is a typical problem in the high magnetic fields regime. (c) We propose a set of protocols where even though the electron spin is driven with a bounded RF, $|\Omega(t)| < \omega_l$, an effective dressed electronic energy gap that is equal to the LF is obtained. The effective electron-nucleus coupling strength decreases for a larger frequency mismatch $\omega_l - \Omega$. Dotted lines (solid lines) indicate energy gaps (driving fields).

where ω_0 corresponds to the NV's energy gap, ω_l is the nucleus LF, σ_z and I_z are the Pauli operators in the direction of the static magnetic field of the NV and the nucleus respectively, g is the NV-nucleus coupling strength, and Ω_1 is the RF of the NV drive. For sensing and control of the nucleus by the NV the HH condition, $\Omega_1 = \omega_l$, must be fulfilled [Fig. 1(a)] [33].

In the high magnetic field regime the nuclear LF, $\omega_l = \gamma_n B$, where γ_n is the nuclear gyromagnetic ratio and B is the static magnetic field, can be as high as ~100 MHz. Hence, because of either technical limitations or avoidance of heating effects that occur due to the high power that is required to generate such a large RF, it is impossible to fulfil the HH condition by an on-resonance drive. Namely, we must work in the regime where $|\Omega_1| < \omega_l$ [Fig. 1(b)]. We term the frequency difference, $\omega_l - \Omega_1$, as the frequency mismatch between the NV frequency (Ω_1) and the nuclear LF (ω_l).

We propose a set of protocols where even though the electron is driven with a bounded RF, $|\Omega(t)| < \omega_l$, an effective dressed electronic energy gap that is equal to the LF is obtained, and hence, the resonance condition is retrieved. Most generally, we consider the Hamiltonian $H_s = (\omega_0/2)\sigma_z + (\omega_l/2)I_z + g\sigma_z I_x + \Omega_1(t)\sigma_x \cos[\phi(t)]$, where $\Omega_1(t)$ and $\phi(t)$ are the modulated RF and modulated phase of a general driving field. The functions $\phi(t)$ and $\Omega_1(t)$ are our control tools that are used in order to reach the resonance condition in the small and large frequency mismatch regimes respectively, and therefore enable us to probe the nuclei parameters and polarize it in the high magnetic field regime.

Small frequency mismatch.—In continuous dynamical decoupling it is more beneficial to rely on a control by a robust phase modulation (PM) than on a control by a noisy amplitude modulation (AM) [37]. This concept was verified experimentally [32,38] and here we further develop it to design efficient and robust control in the high magnetic field regime when the frequency mismatch is small. This scenario is relevant for a LF of ~1–10 MHz. For example, the LF of ^{13}C (^{15}N) at a magnetic field of 1T (1.5T) is 10 MHz (6.5 MHz). There are two key advantages of PM. First, PM is much more stable than a noisy AM and therefore results in longer coherence times. Second, the extra frequency that is required to fulfil the resonance condition ($\omega_l - \Omega_1$) originates only from the PM and therefore does not require extra power beyond the power limit of the bounded RF Ω_1 [33].

We consider the following Hamiltonian of the NV and the nucleus, $H = (\omega_0/2)\sigma_z + \delta B(t)\sigma_z + (\omega_l/2)I_z + g\sigma_z I_x + [\Omega_1 + \delta\Omega_1(t)]\sigma_x \cos[\omega_0 t + 2(\Omega_2/\Omega_1)\sin(\Omega_1 t)]$, where $\delta B(t)$ is the magnetic noise, Ω_1 is the RF of the drive, which defines the PM according to $\phi(t) = 2(\Omega_2/\Omega_1)\sin(\Omega_1 t)$, and $\delta\Omega_1(t)$ is the amplitude noise in Ω_1. The NV dynamics is modulated by two frequencies, Ω_1 and Ω_2, and thus we may expect transitions to occur whenever the resonance condition, $\Omega_1 + \Omega_2 = \omega_l$, is met. Indeed, this Hamiltonian results in double-dressed NV states for which we have that [33] $H_{II} \approx (\Omega_2/2)\sigma_z + (\omega_l/2)I_z - (g/2)[\sigma_+(e^{i\Omega_1 t} - e^{-i\Omega_1 t}) + \sigma_-(e^{-i\Omega_1 t} - e^{i\Omega_1 t})]I_x$, where H_{II} is the Hamiltonian in the second interaction picture (IP) and in the basis of the double-dressed states. From this expression it is seen that a resonance condition appears when $\Omega_1 + \Omega_2 = \omega_l$ (or when $\Omega_1 - \Omega_2 = \omega_l$). Even though the power of the driving field is $\propto \Omega_1^2$ and is independent of Ω_2, higher Larmor frequencies than what is available by the peak power in a common HH scheme are reachable. While the modulation by the frequency Ω_1 originates from AM and requires a power of $\propto \Omega_1^2$, the second modulation by the frequency Ω_2 originates from the PM and as such it is not associated with extra power. Specifically, for $\Omega_2 = \Omega_1$ the ratios of the peak power (the maximal instantaneous power value) and the cycle power [the power that is required for a complete energy transfer (flip flop) between the NV and the nucleus] between a common HH drive and a phase modulated drive are 4 and 2, respectively [33]. Moreover, PM may result in significantly prolonged coherence times due to the precise phase control of microwave sources, and the elimination (to first order) of amplitude fluctuations in Ω_1 [33].

The above procedure is correct in the limit of $\Omega_2 \ll \Omega_1$. However, we aim to increase Ω_2 as much as possible without reducing the sensitivity. To this end, we have to take into account the Bloch-Siegert Shift (BSS) due to the counter-rotating terms of the second modulation Ω_2, which induces a shift of the resonance. In addition, this decreases the coupling to the nucleus, and more importantly, the coherence time of the NV as the decoupling effect of the drive is not effective any more [Fig. 3 (blue)]. To improve this, we suggest correcting the BSS when adjusting the frequency Ω_1 in the PM $\phi(t) = 2(\Omega_2/\Omega_1)\sin(\Omega_1 t)$ and modify it to $\tilde{\Omega}_1 = \frac{1}{3}(\Omega_1 + \sqrt{4\Omega_1^2 + 3\Omega_2^2})$. In this case, the resonance frequency is $\tilde{\Omega}_1 + \tilde{\Omega}_2 = \omega_l$, where $\tilde{\Omega}_2 = (\Omega_2/2)\{1 + [(\Omega_1 + \tilde{\Omega}_1)/\sqrt{\Omega_2^2 + (\Omega_1 + \tilde{\Omega}_1)^2}]\}$ [33].

In Fig. 2 we show simulation results [33] for the nucleus polarization as function of Ω_2/Ω_1. In the main figure we consider the strong coupling regime, where the polarization time $t = 2\pi/g$ is much shorter than the decoherence time of the NV center and hence, decoherence effects are neglected. In the inset we consider the weak coupling regime where noise decreases the polarization rate [33]. We define the nuclear spin polarization, P_N, as the probability of the nuclear spin to be in its initial state $|\uparrow_z\rangle$. Specifically, we initialize the NV-nucleus state to $|\psi_i\rangle = |\downarrow_z\rangle_{\mathrm{NV}}|\uparrow_z\rangle_N = |\downarrow_z\uparrow_z\rangle$ and calculate the polarization according to $P_N = |\langle\uparrow_z\uparrow_z|\psi\rangle|^2 + |\langle\downarrow_z\uparrow_z|\psi\rangle|^2$, where $|\psi\rangle$ is the joint NV-nucleus state at the optimal polarization time. Hence, $P_N = 0$ corresponds to optimal polarization and $P_N = 1$ corresponds to no polarization at all. While in the strong coupling regime the correction always results in better

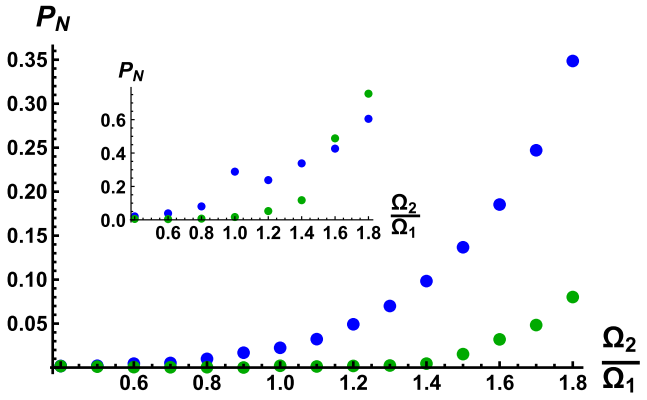

FIG. 2. Polarization as a function of Ω_2/Ω_1 in the strong and weak (inset) coupling regimes without BSS correction (blue) and with BSS correction (green). Strong coupling regime: without correction the polarization rate begins to sharply decrease at $\Omega_2 \approx \Omega_1$. The correction enables us to maintain good polarization rates up to $\Omega_2 \approx 1.8\Omega_1$. Weak coupling regime: The analysis takes noise into account. The polarization is effective up to $\Omega_2 \approx 1.4\Omega_1$.

polarization rates, in the weak coupling regime the advantage of correction is lost at $\Omega_2 \approx 1.5\Omega_1$. In Fig. 3 we show the expected coherence times, T_2, of the NV as a function of Ω_2/Ω_1 [33]. Without the correction the optimal coherence time is sharply peaked at $\Omega_2/\Omega_1 \approx 0.125$ with $T_2 \approx 330$ μs (not shown). The coherence time is reduced when Ω_2 is increased due to an amplitude mixing of $\propto (\Omega_2/\Omega_1)$ between the dressed states, which introduces back a first order contribution of the drive noise $\propto (\Omega_2/\Omega_1)\delta\Omega_1$. This decoherence is greatly mitigated by the correction of the BSS up to $\Omega_2 \approx \Omega_1$, which results in an improvement of 1 order of magnitude in the coherence times. With the correction the optimal coherence time is peaked at

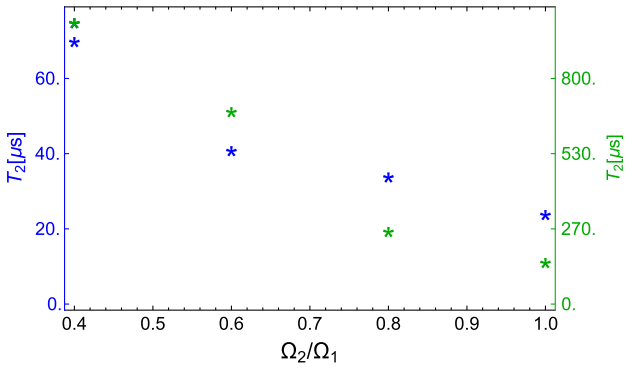

FIG. 3. Coherence time (T_2) as a function of Ω_2/Ω_1. Without the BSS correction (blue), at the regime of an efficient polarization, T_2 is decreased as Ω_2 is increased. The optimal T_2 is sharply peaked at $\Omega_2/\Omega_1 \approx 0.125$ with $T_2 \approx 330$ μs (not shown). With the BSS correction (green), a long T_2 time is maintained while increasing Ω_2. The optimal T_2 is peaked at $\Omega_2/\Omega_1 \approx 0.4$ with $T_2 \approx 1000$ μs. The coherence time is a crucial parameter in the efficiency of control and estimation.

$(\Omega_2/\Omega_1) \approx 0.4$ with $T_2 \approx 1000$ μs. In this case, the coherence time is mainly limited by the second order contribution of the drive noise $\sim(\delta\Omega_1^2/\Omega_2)$. The BSS correction enables us to further increase Ω_2 and results in prolonged NV's coherence times and higher polarization rates.

Large frequency mismatch.—The natural way to compensate for the frequency mismatch is to introduce a detuning (δ) to the drive. This detuning induces an extra modulation that creates an effective frequency of $\sqrt{\Omega_1^2+\delta^2}$, which, in principle, can be as high as needed ($\sqrt{\Omega_1^2+\delta^2} \gg \Omega_1$). When the effective frequency $\sqrt{\Omega_1^2+\delta^2}$ is equal to the LF, the HH condition is fulfilled and the electron-nucleus interaction is enabled [33]. This, however, comes with a price; the electron-nucleus coupling strength is decreased by a factor of $\sim(\Omega_1/\delta)$ [33] [Fig. 1(c)]. Here the decoupling effect of a resonant drive vanishes and the NV's coherence time approaches T_2^*. In [33] we show how to circumvent this by adding a second drive. This scheme, however, could be extremely power efficient; e.g., for $\delta = 10\Omega_1$ the ratios of the peak power and the cycle power between a common HH drive and a detuned drive are 101 and 10.1, respectively [33].

An alternative way to reach the resonance is to modulate the amplitude of the drive. This AM generates higher harmonics of the modulation frequency that can be tuned to be on resonance with the LF. We start with the Hamiltonian $H = (\omega_0/2)\sigma_z + (\omega_l/2)I_z + g\sigma_z I_x + \Omega(t)\sigma_x \cos(\omega_0 t)$ and set $\Omega(t) = \Omega_0 + \Omega_1 \cos(\Omega_2 t)$. Moving to the IP with respect to $H_0 = (\omega_0/2)\sigma_z$ and making the rotating-wave approximation (RWA) ($\omega_0 \gg |\Omega(t)|$) we obtain $H_I = [\Omega(t)/2]\sigma_x + (\omega_l/2)I_z + g\sigma_z I_x$, which in the basis of the NV dressed states ($x \to z$, $z \to -x$, and $y \to y$) is given by $H_I = [\Omega(t)/2]\sigma_z + (\omega_l/2)I_z - g\sigma_x I_x$. We continue by moving to the second IP with respect to $H_0 = [\Omega(t)/2]\sigma_z + (\omega_l/2)I_z$, which results in $H_{II} = -g(\sigma_+ e^{i[\Omega_0 t + (\Omega_1/\Omega_2)\sin(\Omega_2 t)]} + \text{H.c.}) \times (I_+ e^{i\omega_l t} + I_- e^{-i\omega_l t})$. The exponent $e^{i[\Omega_0 t + (\Omega_1/\Omega_2)\sin(\Omega_2 t)]}$ contains the higher harmonics of Ω_2, i.e., $n\Omega_2$, where n is an integer. This can be seen by the equality $e^{i[\Omega_0 t + (\Omega_1/\Omega_2)\sin(\Omega_2 t)]} = e^{i\Omega_0 t}\sum_{n=-\infty}^{n=+\infty}[i^n J_n(\Omega_1/\Omega_2)e^{in\Omega_2 t} + \text{H.c.}]$. We can therefore set the resonance condition to $\Omega_0 + \Omega_2 = \omega_l$. Assuming the RWA ($\Omega_2 \gg g$) we get that $H_{II} \approx gJ_1(\Omega_1/\Omega_2)(i\sigma_+ I_- - i\sigma_- I_+)$ when the resonance condition is fulfilled. In the regime of $\Omega_2 \gg \Omega_1$, $J_1(\Omega_1/\Omega_2) \approx (\Omega_1/2\Omega_2)$. Hence, the coupling strength is similar to the one in the previous method; however, this scheme is robust to magnetic noise. Numerical analysis of this method is shown in Fig. 4. With a single AM the method suffers from amplitude fluctuations in Ω_0, which could be eliminated by realizing this as a second drive from a PM [33]. This scheme is also power efficient; e.g., for $\Omega_2 = 9\Omega_0$ the ratios of the peak power and the cycle power between a common HH drive and an amplitude modulated drive are 25 and 3.7, respectively [33].

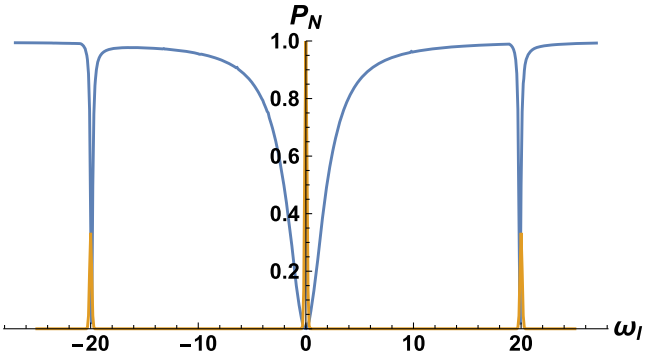

FIG. 4. Polarization as a function of the nuclear LF in units of tenth of the coupling strength (blue line). The central resonance corresponds to $\omega_l = \Omega_0$. The two sidebands correspond to $\omega_l = \Omega_0 \pm \Omega_2$. The y axis corresponds to the occupation of the nucleus when the initial state is the $|\uparrow_z\rangle$ state, i.e., $P_N = 1$. The main deep is broader than the side deeps because the coupling at the sideband frequencies is reduced. In contrast, the yellow line represent the analysis of the quantum sensing Hamiltonian, which is much narrower and is not limited by the coupling strength. The numerical simulations were performed with $\Omega_0 = 1.5$ MHz, $\Omega_1 = 0.1$ MHz, $\Omega_2 = 1$ MHz, and $g = 0.05\Omega_2$.

Quantum sensing.—Addressability is the ability of a probe to individually address and control nuclear spins, which was discussed above. However, addressability is not necessary for quantum sensing where, e.g., one is only interested in estimating the LF, as in nano-NMR experiments. The resolution of addressability is defined by the ability to control a nucleus with a given frequency ω_l, while leaving nuclei with different frequencies outside of a frequency width $\Delta\omega$ (centered at ω_l) unaffected. As shown in Fig. 4 in blue, the addressability resolution is limited by the coupling strength. This is because all frequencies within a width of the coupling strength from the resonance will couple to the probe. Hence, the stronger the coupling the worse the resolution, and a larger band of frequencies will be addressed by the probe.

However, when the NV is used to estimate the LF, one would expect that the stronger the coupling the more information acquired; an increased coupling strength should improve the resolution and not limit it. The addressability resolution limit could be overcome by designing the Hamiltonian differently. In cases that control is not necessary, and one is just interested in frequency estimation of the nuclei, methods that are not limited by the coupling strength could be designed. The difference between the methods is analogous to the difference between Rabi and Ramsey spectroscopy. While power is a limiting factor in the first method (necessitating weak pulses), it poses no limitation in the second method.

The addressability resolution problem occurs as the NV coupling operator term is a $\sigma_\pm$ operator that is in charge of energy transfer. This is crucial for control; however, it is not needed for sensing. An interaction of the addressability type, $g(\sigma_- I_+ + \sigma_+ I_-)$, transfers excitations between the two spins as long as their frequency difference is smaller than the coupling strength g. Thus, the target frequencies within a spread of g are addressed by the probe. However, an interaction of the type $g\sigma_x(I_+ + I_-) = g\sigma_x I_x$ could be utilized to estimate the frequencies of the target spins with a resolution that is not limited by the coupling strength [39–41]. This can be achieved by transforming the σ_-, σ_+ operators into a σ_x (or σ_y) operator, which is doable as $\sigma_\pm = \sigma_x \pm i\sigma_y$ and σ_y could be eliminated with a suitable control, e.g., by adding a strong σ_x drive that eliminates the σ_y part. For the case of the low-frequency mismatch this can be achieved by adding an extra drive on the NV, which rotates at Ω_2 [this amounts to $\Omega_s \cos(\omega_0 t)\cos(\Omega_2 t)\sigma_x$]. In [33] we explicitly show that this results in an Hamiltonian that can be used for sensing the LF, i.e., $H_I \approx (g/4) \times \sigma_z[I_x \cos(\delta t) - I_y \sin(\delta t)]$, where $\delta = \Omega_1 + \Omega_2 - \omega_l$. As the extra term acts as a spin locking at Ω_s, the robustness of the methods is preserved. The classical version of this Hamiltonian was used in [39–48] where it was shown that the resolution is only limited by the clock and signal coherence times. The resolution obtained by this Hamiltonian, which is the generic sensing Hamiltonian, is only limited by the coherence time of the nuclei and the sensitivity is improved with the coupling strength [49].

The same can be done in the large frequency mismatch regime. The interaction should be changed from the flip-flop interaction $g(\sigma_+ I_- + \sigma_- I_+)$ to $g\sigma_x I_x$ by adding, e.g., a σ_x drive to the modulation. In this case the Hamiltonian is transformed to [33] $H \approx gJ_1(\Omega_1/\Omega_2)\sigma_x[I_x \cos(\delta t) - I_y \sin(\delta t)]$. The result of using this Hamiltonian for estimating the nuclei's frequencies is shown in Fig. 4. The yellow line is the Fourier transform of the time series of NV measurements for a scenario in which a few nuclei are present at the three frequencies $\Omega_0, \Omega_0 \pm \Omega_1$. The width of these peaks (one over the total experiment time) is narrower than the peaks of the control method (blue line), which is limited by the coupling strength.

The challenge of controlling and sensing high-frequency nuclei under power limitations of the driving fields was addressed both in the small and large frequency mismatch regimes. We have designed schemes that are robust both to magnetic field fluctuations and RF noise. The presented protocols could potentially allow for the realization of experiments in an important regime that is currently out of reach and could considerably simplify state of the art experiments.

Acknowledgements

A. R. acknowledges the support of ERC grant Quantum Resolution (QRES), Grants No. 770929 and No. 667192 (Hyperdiamond), the Microwave Quantum Computation (MicroQC), the Advancing Science and TEchnology thRough dIamond Quantum Sensing (ASTERIQS), and the Diamond Polarizarion (DiaPol) project.

Note added.—Recently we became aware of a related independent work by Casanova *et al.* [50].

[1] F. Jelezko and J. Wrachtrup, Phys. Status Solidi (a) **203**, 3207 (2006).

[2] S.-Y. Lee, M. Widmann, T. Rendler, M. W. Doherty, T. M. Babinec, S. Yang, M. Eyer, P. Siyushev, B. J. Hausmann, M. Loncar *et al.*, Nat. Nanotechnol. **8**, 487 (2013).

[3] P. Neumann, J. Beck, M. Steiner, F. Rempp, H. Fedder, P. R. Hemmer, J. Wrachtrup, and F. Jelezko, Science **329**, 542 (2010).

[4] M. Pfender, P. Wang, H. Sumiya, S. Onoda, W. Yang, D. B. R. Dasari, P. Neumann, X.-Y. Pan, J. Isoya, R.-B. Liu *et al.*, Nat. Commun. **10**, 594 (2019).

[5] T. Unden, P. Balasubramanian, D. Louzon, Y. Vinkler, M. B. Plenio, M. Markham, D. Twitchen, A. Stacey, I. Lovchinsky, A. O. Sushkov, M. D. Lukin, A. Retzker, B. Naydenov, L. P. McGuinness, and F. Jelezko, Phys. Rev. Lett. **116**, 230502 (2016).

[6] L. Jiang, J. Hodges, J. Maze, P. Maurer, J. Taylor, D. Cory, P. Hemmer, R. Walsworth, A. Yacoby, A. Zibrov *et al.*, Science **326**, 267 (2009).

[7] M. G. Dutt, L. Childress, L. Jiang, E. Togan, J. Maze, F. Jelezko, A. Zibrov, P. Hemmer, and M. Lukin, Science **316**, 1312 (2007).

[8] A. L. Falk, P. V. Klimov, V. Ivády, K. Szász, D. J. Christle, W. F. Koehl, Á. Gali, and D. D. Awschalom, Phys. Rev. Lett. **114**, 247603 (2015).

[9] V. Ivády, K. Szász, A. L. Falk, P. V. Klimov, D. J. Christle, E. Janzén, I. A. Abrikosov, D. D. Awschalom, and A. Gali, Phys. Rev. B **92**, 115206 (2015).

[10] J. J. Morton, A. M. Tyryshkin, R. M. Brown, S. Shankar, B. W. Lovett, A. Ardavan, T. Schenkel, E. E. Haller, J. W. Ager, and S. Lyon, Nature (London) **455**, 1085 (2008).

[11] J. J. Pla, K. Y. Tan, J. P. Dehollain, W. H. Lim, J. J. Morton, F. A. Zwanenburg, D. N. Jamieson, A. S. Dzurak, and A. Morello, Nature (London) **496**, 334 (2013).

[12] N. Y. Yao, L. Jiang, A. V. Gorshkov, P. C. Maurer, G. Giedke, J. I. Cirac, and M. D. Lukin, Nat. Commun. **3**, 800 (2012).

[13] L. Childress and R. Hanson, MRS Bull. **38**, 134 (2013).

[14] L. Robledo, L. Childress, H. Bernien, B. Hensen, P. F. Alkemade, and R. Hanson, Nature (London) **477**, 574 (2011).

[15] T. Van der Sar, Z. Wang, M. Blok, H. Bernien, T. Taminiau, D. Toyli, D. Lidar, D. Awschalom, R. Hanson, and V. Dobrovitski, Nature (London) **484**, 82 (2012).

[16] T. H. Taminiau, J. Cramer, T. van der Sar, V. V. Dobrovitski, and R. Hanson, Nat. Nanotechnol. **9**, 171 (2014).

[17] N. Aslam, M. Pfender, R. Stöhr, P. Neumann, M. Scheffler, H. Sumiya, H. Abe, S. Onoda, T. Ohshima, J. Isoya *et al.*, Rev. Sci. Instrum. **86**, 064704 (2015).

[18] V. S. Perunicic, L. T. Hall, D. A. Simpson, C. D. Hill, and L. C. L. Hollenberg, Phys. Rev. B **89**, 054432 (2014).

[19] X. Kong, F. Shi, Z. Yang, P. Wang, N. Raatz, J. Meijer, and J. Du, Phys. Rev. B **97**, 205438 (2018).

[20] F. Shagieva, S. Zaiser, P. Neumann, D. B. R. Dasari, R. Sthr, A. Denisenko, R. Reuter, C. A. Meriles, and J. Wrachtrup, Nano Lett. **18**, 3731 (2018).

[21] D. Pagliero, K. K. Rao, P. R. Zangara, S. Dhomkar, H. H. Wong, A. Abril, N. Aslam, A. Parker, J. King, C. E. Avalos *et al.*, Phys. Rev. B **97**, 024422 (2018).

[22] D. A. Broadway, J.-P. Tetienne, A. Stacey, J. D. Wood, D. A. Simpson, L. T. Hall, and L. C. Hollenberg, Nat. Commun. **9**, 1246 (2018).

[23] P. Fernández-Acebal, O. Rosolio, J. Scheuer, C. Mller, S. Mller, S. Schmitt, L. McGuinness, I. Schwarz, Q. Chen, A. Retzker *et al.*, Nano Lett. **18**, 1882 (2018).

[24] J. Scheuer, I. Schwartz, Q. Chen, D. Schulze-Sünninghausen, P. Carl, P. Höfer, A. Retzker, H. Sumiya, J. Isoya, B. Luy *et al.*, New J. Phys. **18**, 013040 (2016).

[25] Q. Chen, I. Schwarz, F. Jelezko, A. Retzker, and M. B. Plenio, Phys. Rev. B **93**, 060408 (2016).

[26] S. Hartmann and E. Hahn, Phys. Rev. **128**, 2042 (1962).

[27] T. Häberle, T. Oeckinghaus, D. Schmid-Lorch, M. Pfender, F. F. de Oliveira, S. A. Momenzadeh, A. Finkler, and J. Wrachtrup, Rev. Sci. Instrum. **88**, 013702 (2017).

[28] V. Stepanov, F. H. Cho, C. Abeywardana, and S. Takahashi, Appl. Phys. Lett. **106**, 063111 (2015).

[29] M. Pfender, N. Aslam, P. Simon, D. Antonov, G. Thiering, S. Burk, F. Fvaro de Oliveira, A. Denisenko, H. Fedder, J. Meijer *et al.*, Nano Lett. **17**, 5931 (2017).

[30] J. Casanova, Z.-Y. Wang, I. Schwartz, and M. Plenio, Phys. Rev. Applied **10**, 044072 (2018).

[31] G. Gordon, G. Kurizki, and D. A. Lidar, Phys. Rev. Lett. **101**, 010403 (2008).

[32] Q.-Y. Cao, Z.-J. Shu, P.-C. Yang, M. Yu, M.-S. Gong, J.-Y. He, R.-F. Hu, A. Retzker, M. Plenio, C. Müller *et al.*, arXiv:1710.10744.

[33] See Supplemental Material at http://link.aps.org/supplemental/10.1103/PhysRevLett.122.120403 for detailed derivations of the results that appear in the main text, which includes Refs. [34–36].

[34] C. Cohen-Tannoudji, B. Diu, and F. Laloe, *Quantum Mechanics*, edited by C. Cohen-Tannoudji, B. Diu, and F. Laloe (Wiley-VCH, New York, 1986), Vol. 2, p. 626.

[35] D. T. Gillespie, Phys. Rev. E **54**, 2084 (1996).

[36] N. Aharon, I. Cohen, F. Jelezko, and A. Retzker, New J. Phys. **18**, 123012 (2016).

[37] I. Cohen, N. Aharon, and A. Retzker, Fortschr. Phys. **65**, 1600071 (2017).

[38] D. Farfurnik, N. Aharon, I. Cohen, Y. Hovav, A. Retzker, and N. Bar-Gill, Phys. Rev. A **96**, 013850 (2017).

[39] S. Schmitt, T. Gefen, F. M. Stürner, T. Unden, G. Wolff, C. Müller, J. Scheuer, B. Naydenov, M. Markham, S. Pezzagna *et al.*, Science **356**, 832 (2017).

[40] D. B. Bucher, D. R. Glenn, J. Lee, M. D. Lukin, H. Park, and R. L. Walsworth, arXiv:1705.08887.

[41] J. Boss, K. Cujia, J. Zopes, and C. Degen, Science **356**, 837 (2017).

[42] A. Laraoui, F. Dolde, C. Burk, F. Reinhard, J. Wrachtrup, and C. A. Meriles, Nat. Commun. **4**, 1651 (2013).

[43] S. Zaiser, T. Rendler, I. Jakobi, T. Wolf, S.-Y. Lee, S. Wagner, V. Bergholm, T. Schulte-Herbrüggen, P. Neumann, and J. Wrachtrup, Nat. Commun. **7**, 12279 (2016).

[44] T. Staudacher, N. Raatz, S. Pezzagna, J. Meijer, F. Reinhard, C. Meriles, and J. Wrachtrup, Nat. Commun. **6**, 8527 (2015).
[45] A. Ajoy, U. Bissbort, M. D. Lukin, R. L. Walsworth, and P. Cappellaro, Phys. Rev. X **5**, 011001 (2015).
[46] T. Rosskopf, J. Zopes, J. Boss, and C. Degen, arXiv: 1610.03253.
[47] A. Laraoui, J. S. Hodges, C. A. Ryan, and C. A. Meriles, Phys. Rev. B **84**, 104301 (2011).
[48] M. Pfender, N. Aslam, H. Sumiya, S. Onoda, P. Neumann, J. Isoya, C. Meriles, and J. Wrachtrup, Nat. Commun. **8**, 834 (2017).
[49] T. Gefen, M. Khodas, L. P. McGuinness, F. Jelezko, and A. Retzker, Phys. Rev. A **98**, 013844 (2018).
[50] J. Casanova, E. Torrontegui, M. B. Plenio, J. J. García-Ripoll, and E. Solano, Phys. Rev. Lett. **122**, 010407 (2019).